Climatic and tectonic controls on source-to-sink processes in the tropical, ultramafic catchment of Lake Towuti, Indonesia

Marina A. Morlock[a,*], Hendrik Vogel[a], Valentin Nigg[a], Luis Ordoñez[b], Ascelina K. M. Hasberg[c], Martin Melles[c], James M. Russell[d], Satria Bijaksana[e] & the TDP Science Team

[a]Institute of Geological Sciences and Oeschger Centre for Climate Change Research, University of Bern, 3012 Bern, Switzerland

[b]Department of Earth Sciences, University of Geneva, 1205 Geneva, Switzerland

[c]Institute of Mineralogy and Geology, University of Cologne, 50674 Cologne, Germany

[d]Department of Earth, Environmental, and Planetary Sciences, Brown University, Providence RI 02912, USA

[e]Faculty of Mining and Petroleum Engineering, Institut Teknologi Bandung, Bandung 40132, Indonesia

* corresponding author: marina.morlock@geo.unibe.ch

Email addresses:

marina.morlock@geo.unibe.ch (M.A. Morlock), hendrik.vogel@geo.unibe.ch (H. Vogel), valentin.nigg@geo.unibe.ch (V. Nigg), Luis.Ordonez@unige.ch (L. Ordoñez), hasberga@uni-koeln.de (A.K.M. Hasberg), mmelles@uni-koeln.de (M. Melles), james_russell@brown.edu (J. M. Russell), satria@fi.itb.ac.id (S. Bijaksana)

Keywords

Laterite, Erosion, Hydroclimate, Lake Towuti, Lake level, Tropical palaeoclimate

Abstract

Humid tropical landscapes are subject to intense weathering and erosion, which strongly influence sediment mobilisation and deposition. In this setting, we aimed to understand how geomorphology and hydroclimate altered the style and intensity of erosion and sediment composition in a tropical lake and its tectonically active catchment. Lake Towuti (2.75°S, 121.5°E) is one of the oldest and deepest lakes in Indonesia, with uninterrupted lacustrine sedimentation over several glacial-interglacial cycles. Here we present results from a novel set of Lake Towuti surface sediment, bedrock and soil samples from the catchment, and two existing sediment cores that extend to 30,000 and 60,000 years before present. We studied the catchment morphology, soil properties, geochemistry, and clay and bulk mineralogy. Results from several river long profiles show clear signs of tectonic activity, which enhances river incision, favours mass movement processes, and together with remobilisation of fluvial deposits, strongly influences modern sedimentation in the lake. Material from the Mahalona River, the lake's largest inflow, dominates modern sediment composition in Towuti's northern basin. The river transports Al-poor and Mg-rich sediments (mainly serpentines) to the lake, indicating river incision into the Mg-rich serpentinised peridotite bedrock. Relatively small, but important additional contributions of material, come from direct laterite-derived input and the Loeha River, which both provide Al-rich and Mg-poor sediment to the lake. Over time, the Al/Mg and kaolinite-to-serpentine ratios varied strongly, primarily in response to lake-level fluctuations driven by hydroclimatic changes. In the past 60,000 years, both the Al/Mg and kaolinite-

to-serpentine ratios showed variations sensitive to changes in climate boundary conditions across glacial-interglacial cycles, while tectonic activity had less influence on changes in sediment composition on these short time-scales.

Introduction

In the humid tropics, intense weathering results in a thick soil cover that is very susceptible to erosion by mass-wasting and high rainfall events. Soils provide an important resource for economic development in many (tropical) countries, both for agricultural use and mineral exploitation (U.S. Geological Survey 2017). Specifically, laterites are autochthonous weathering products characterised by high concentrations of immobile elements such as Fe and Al in the upper soil horizons (Widdowson 2007). There are several studies of laterite properties in tropical Africa (Ogunsanwo 1988; Omotoso et al. 2012; Adunoye 2014), but there is little known about how laterite properties influence erosion and sedimentary processes. Similarly, although a number of studies described the laterization of ultramafic bedrock (Golightly and Arancibia 1979; Colin et al. 1990; Brand et al. 1998; Sagapoa et al. 2011; Marsh et al. 2013), these studies often focused on ore exploration. The interaction between climate, soil properties, catchment geomorphology, and sedimentary processes has rarely been explored in laterite landscapes, and in the humid tropics in general.

77 Equatorial Lake Towuti (2.75°S, 121.5°E, 560 km^2, ~200 m maximum
78 water depth; Fig. 1) is one of the oldest lakes in Indonesia (Von Rintelen et al.
79 2012). The catchment geology consists of dunites, lherzolites, and
80 harzburgites of the East Sulawesi Ophiolite complex (Kadarusman et al.
81 2004), upon which thick laterites have developed. Particles and solutes
82 delivered to the lake are exceptionally rich in iron, but very poor in sulphur and
83 macronutrients, setting the stage for unusual biogeochemical cycles,
84 ultraoligotrophy, and a highly adapted, mostly endemic lake fauna and flora
85 (Haffner et al. 2001; Crowe et al. 2008; Von Rintelen et al. 2012). Most of the
86 lake is surrounded by dense, closed-canopy rainforest; however, based on
87 satellite images, ~25% of the lake catchment is now deforested as a
88 consequence of anthropogenic activities. Previous studies of Lake Towuti
89 suggest that during the past 60,000 years, hydrologic changes driven by
90 changing global climate boundary conditions had large impacts on lake
91 sedimentation (Russell et al. 2014; Vogel et al. 2015). Lake-level lowstands
92 were accompanied by delta progradation into the deeper basins, which
93 favours lateral transport processes relative to pelagic sedimentation (Vogel et
94 al. 2015). This change in depositional modes leads to coarser-grained
95 sediments in the deeper basins and associated changes in mineralogy
96 (Weber et al. 2015; Goudge et al. 2017). In 2015 the International Continental
97 Scientific Drilling Program (ICDP) Towuti Drilling Project (TDP) recovered
98 cores through the entire sediment infill of Lake Towuti which record
99 uninterrupted lacustrine sedimentation over several glacial-interglacial cycles
100 (Russell et al. 2016).
101

We carried out novel analyses of bedrock and soil samples from Lake Towuti's catchment, along with geomorphological analyses, to characterise and understand modern source-to-sink processes around this tropical lake system. We analysed the inorganic geochemistry, clay and bulk mineralogy, and sedimentological characteristics of bedrock, soils, and lake surface sediment and core samples to disentangle the effects of climatic and tectonic processes and their influence on erosion and sedimentation. We applied this understanding to interpret mineralogical and geochemical variations in two sediment cores that extend 30 and 60 kilo years before present (kyr BP). This study links modern sedimentation processes to existing and new palaeoclimate reconstructions from Lake Towuti to better understand modern tropical lake systems and how such systems change under different climate boundary conditions. Such a study is timely, given the unprecedented rates of anthropogenically induced change that tropical regions are currently undergoing.

Hydrologic setting

Lake Towuti is part of the Malili Lake System, a chain of five tectonic lakes located on the island of Sulawesi, Indonesia (Fig. 1). The lake receives annual precipitation of ~2700 mm, with peak rainfall (~330 mm/month) in austral autumn (MAM), and comparatively dry (~140 mm/month) austral spring months (ASO; Konecky et al. 2016). Lake Towuti is a hydrologically open lake with one outflow, the Larona River (Fig. 1c). The lake is split into two connected major basins to the north and south (Figs. 1c and 2), which are

127 separated by bedrock highs above and below the current water surface
128 (Vogel et al. 2015; Russell et al. 2016). To the north, the lake is connected to
129 upstream Lakes Matano and Mahalona via the Mahalona River (Fig. 1d),
130 which dominates water and sediment input to Towuti's northern basin (Costa
131 et al. 2015). The large catchment of the Mahalona River includes the
132 Lampenisu River catchment, which is characterised by Quaternary alluvium
133 and partly serpentinised peridotites. Together, the two rivers comprise 25%
134 (293 km^2) of the catchment area of Lake Towuti, excluding the catchments of
135 Lakes Matano and Mahalona. Despite severe drying during the last glacial
136 maximum (Russell et al. 2014) and associated lake-level lowstands, the lake
137 remained hydrologically connected to upstream lakes via the Mahalona River
138 throughout the last 60,000 years (Costa et al. 2015). Lake Towuti's southern
139 basin has four prominent inflows. The Loeha River drains a catchment hosting
140 metasedimentary rock to the east of the lake, the only source of felsic
141 minerals in the catchment of Lake Towuti (Fig. 1b and d, Costa et al. 2015).
142 Three rivers at the southern tip of the lake jointly drain 10% of the lake's
143 catchment and are underlain by ultramafic rocks. Lake Towuti's western and
144 northeastern shores are dominated by steep slopes and densely vegetated
145 catchments with no major permanent river drainage (Fig. 1d).
146
147 **Materials and methods**
148
149 Geotechnical and geomorphological analysis
150

River and catchment morphology were analysed using a digital elevation model (DEM) of the Lake Towuti region. The DEM is based on data from NASA's Shuttle Radar Topography Mission at 1 arc-second (30 m) spatial resolution (available at: http://earthexplorer.usgs.gov, last accessed: February 09 2017). Rivers and catchment boundaries were identified using the hydrology toolset in ArcGIS 10.1 (Esri, USA). Catchment sizes, river lengths, trunk channel relief, and long profiles were calculated based on this DEM data set.

In total, 18 bedrock samples (from 12 locations) and 6 laterite profiles (21 samples) were collected in May-July 2015 (Fig. 1c). Samples cover varying degrees of serpentinisation of the peridotite bedrock and represent all the vertical zones of the laterites. Because of accessibility, all samples were taken northwest of the lake (Fig. 1c). Representative laterite samples, formed on serpentinised and non-serpentinised peridotites, were dried at 110°C overnight and their plasticity index (I_p), grain-size distributions, soil cohesion (c), and friction angle (angle of internal friction φ) were determined at the geotechnical laboratory of the Bern University of Applied Sciences in Burgdorf, Switzerland. Grain-size data were acquired following Swiss norms SN 670 816a and SN 670 902-1. Samples were treated with 15 ml $Na(PO_3)_6$ for 24 h before settling, wet, and dry sieving. The resulting grain-size distribution curves were categorized following the Unified Soil Classification System and corresponding geotechnical parameters were selected according to Swiss Norm SN 670 010. The parameters φ and c were determined in repeated direct shearing tests, for which varying loads (20, 40, and 80 kN)

were applied to the samples for 20 h before samples were sheared at a rate of 1 mm per minute under undrained conditions (German Industrial Norm DIN 18137-1 and DIN 18137-3). To calculate the plasticity index, plastic and liquid limits of samples were determined following Swiss Norm SN 670 345b, which follows Casagrande (1932).

Surface sediment collection and sediment coring

In 2015, 84 surface sediment samples from across the entire lake were recovered from water depths between 2.8 and 195.5 m with a grab sampler. Samples integrate the uppermost 3-5 cm of recovered sediment, representing 200-250 yr of sediment accumulation in the deep basins (Russell et al. 2014; Vogel et al. 2015). Core Co1230 (19.8 m long, base ^{14}C-dated to 27 kyr BP) was recovered from a distal position to the Mahalona River Delta in the northern basin at ~203 m water depth in 2010 (Vogel et al. 2015). Core IDLE-TOW10-9B-1K (hereafter TOW9) was recovered from 154 m water depth. This 11.5-m core was dated to ~45 kyr BP by ^{14}C dating at 8.95 m depth, and the sedimentation rate over this interval was extrapolated to an age of 60 kyr BP for the core base (Russell et al. 2014).

Geochemistry and grain size

The geochemical composition of bedrock, laterite, lake surface sediment samples, and sediment samples from core Co1230 was determined by inductively coupled plasma mass spectrometry (ICP-MS) after full acid

digestion (HF, HCl, HNO_3, $HClO_4$) of the samples at the Activation Laboratories Ltd. in Ontario, Canada. Because detection limits were reached for many elements in bedrock and laterite samples, these samples were also measured with wavelength dispersive X-ray fluorescence (WD-XRF), and results are reported for concentrations of K, Mg, Cr, and Ni. For WD-XRF analysis, samples were ground in an oscillating tungsten-carbide mill, dried in an oven at 100°C for 12 h, and heated to 1050°C for two hours. Of the burnt rock powder 1.2121 g were mixed with 6.0000 g of lithium-tetraborate ($Li_2B_4O_7$), placed in a Pt-Au crucible and melted in a Bead Machine (Perl X'3) at 1250°C. Major element concentrations were analysed on a Philips PW2400 WD-XRF spectrometer at the University of Lausanne, Switzerland. The lower detection limit is 0.01 weight-% (wt-%) for all elements. The geochemical composition of the bedload of eight rivers is available from Costa et al. (2015), and Goudge et al. (2017) provide grain-size specific chemical and mineralogical data on bedload and suspended load for the Mahalona River. Geochemistry of sediment core TOW9 is available from Russell et al. (2014).

Based on the ICP-MS measurements, we calculated the Chemical Index of Alteration (CIA) of Nesbitt and Young (1982) as a measure of the degree of chemical weathering of different samples. The index is based on the relative accumulation of the less mobile Al_2O_3 relative to more easily soluble Na_2O, K_2O, and $CaO_{silicate}$ in a weathered substrate, e.g. bedrock, soil or sediment. Because calcareous rocks are largely absent in the catchment of Lake Towuti and petrographic observations do not indicate the presence of detrital $CaCO_3$, we assumed all CaO in the system is derived from silicate

rocks ($CaO_{silicate}$). Grain-size measurements of sediment core Co1230 are available from Vogel et al. (2015), who analysed the samples on a laser diffractometer (Malvern Mastersizer 2000S). The grain-size distribution of lake surface sediments was measured at the University of Cologne, Germany, with a Beckman Coulter LS13320 laser diffractometer. Samples were treated with 15 ml H_2O_2 (30%), 10 ml HCl (10%) and NaOH (1 M) prior to analysis.

Bulk and clay mineralogy

One representative laterite profile over both serpentinised and unserpentinised peridotite bedrock, respectively, was analysed for bulk mineralogy by x-ray diffraction (XRD) on a PANalytical Cubix^3 goniometer with a Cu-tube and a monochromator (45 kV, 40 mA, 5-60° 2θ). The bulk mineralogy of a lake surface sediment transect from the Mahalona River mouth to coring site TOW9 was determined by XRD on a PANalytical X'Pert Pro with a Cu x-ray tube (40 kV, 40 mA, 5-60° 2θ). Prior to analysis, freeze-dried samples were mixed and homogenized with 10 wt-% LiF to provide a standard for peak integration and quantification. Additionally, thin sections of bedrock and saprolite zone samples were examined with a polarizing light microscope.

Clay mineralogical analyses were performed on all sediment samples. The < 2-µm size fraction (clay size) was separated from the sample by Atterberg separation (Robinson 1922; ~0.5 g of sample, 4.5-h settling time, 6-cm settling height, 21°C). For XRD analyses on oriented clay mounts, the clay

fraction was added to three glass plates and dried overnight. One glass plate was measured immediately on a Phillips PW1830 Goniometer (40 kV, 30 mA, 2-40° 2θ), another plate was kept in an ethylene-glycol-saturated atmosphere for at least 48 h prior to measurement, and one plate was heated at 550°C for 1.5 h before measurement (Electronic Supplementary Material [ESM] Fig. S1a). By comparing the three treatment spectra, we identified characteristic peaks for smectites (5.2° 2θ), illite (8.8° 2θ), serpentines (12.24° 2θ), and kaolinite (12.5° 2θ) in the ethylene-glycol-saturated spectrum (ESM Fig. S1a). Kaolinite and serpentine peaks were separated using peak separation software (MacDiff, R. Petschick, Frankfurt, Germany, 2001), the output being peak height in absolute counts. Only selected XRD measurements were done for the highly cemented laterite samples. To further evaluate the interpretation and separation of kaolinite from serpentine minerals by XRD analysis, clay separates of core Co1230 and all bulk samples were also measured by mid-infrared (MIR) Fourier-Transform-Infrared-Spectroscopy (FTIRS). For this, 0.011 ± 0.0001 g of freeze-dried material was mixed with 0.5 ± 0.0005 g of spectroscopic grade KBr and homogenised for at least three minutes. FTIRS analyses were performed at the University of Bern, Switzerland, using a Bruker Vertex 70 equipped with an HTS-XT accessory unit, a liquid nitrogen cooled MCT (Mercury-Cadmium-Telluride) detector, and a KBr beam splitter, in the wavenumber range 3750-520 cm^{-1} at a resolution of 4 cm^{-1}. All measurements were performed in diffuse reflectance mode. Several mineral-characteristic absorbance peaks appear as prominent features in the Towuti samples. Diagnostic peaks for kaolinite were centred at 692, 913, 3620 cm^{-1}, caused by translational, librational, and stretching vibrations of OH groups,

respectively, in kaolinite group minerals (Chester and Elderfield 1973; Farmer 1974; Madejová 2003; Chukanov 2014). Identified absorbance peaks diagnostic for serpentine group minerals were centred at 640, 958, and 3685 cm^{-1}, caused by bending, libration, and stretching vibrations of OH, respectively (Farmer 1974; Madejová 2003; Chukanov 2014). Peak integrals of diagnostic peaks are highly correlated for the individual mineral groups, emphasizing that absorbance in the analysed regions is diagnostic for the respective mineral group, without significant bias from other phases absorbing in the same region (Chester and Elderfield 1973). For further analysis, peak areas with highest correlation to clay XRD and geochemical composition were chosen. These were peaks at wavenumbers 900.8-924.6 cm^{-1} for kaolinite and 3674.9-3694.2 cm^{-1} for serpentine.

Statistics and data analysis

All statistical analyses were performed in R (R Development Core Team 2008). For Pearson correlation tests, normality of the variables was tested with the Shapiro-Wilks test. If the data were not normally distributed, Spearman's rank correlation was used to test for correlations. Statistical parameters are given as mean and one standard deviation. All maps were created in ArcGIS 10.1 (Esri, USA). Unless otherwise stated, interpolation of the surface sediment measurements is based on Kriging (Gaussian process regression) with a fixed radius of 5 km and a minimum of 5 data points used for calculations. Raster size is 50 x 50 m. A geometrical classification was chosen for data visualisation.

Results

Catchment morphology

The three connected lakes of the Malili Lake System (excluding its two satellite lakes) drain a hydrologic catchment area of 2430 km^2. Upstream lakes and their surroundings account for a catchment area of 1286 km^2. We assume that Lakes Matano and Mahalona function as sediment traps, providing water, but little sediment, leaving an area of 1144 km^2 to supply the majority of sediment to Lake Towuti (ESM Table S1). Rivers drain 86% of Towuti's catchment (excluding upstream lake catchments), whereas 14% of the area may be drained by surface runoff and/or ephemeral streams, or is left undrained. The catchments around Lake Towuti have mean slope angles between 13.1° and 16.8° (Fig. 2, ESM Table S1). The trunk channel relief (as defined by Whipple et al. 1999) varies between 150 and 680 m over distances from 5 to 43 km. Excluding the catchments that feed into upstream Lakes Matano and Mahalona, the Mahalona River drains the largest catchment (293 km^2 catchment size, 43 km length, 14.5° average catchment slope), the majority of which consists of the Lampenisu River, followed by the Timampu River (141 km^2 catchment size, 18 km length, 13.1° average catchment slope) and the Loeha River (84 km^2 catchment size, 21 km length, 15.5° average catchment slope). Several knickpoints are present in the river courses to the east of Lake Towuti (Fig. 2). Most prominent, the Loeha River drops by 400 m over a distance of 2.5 km (average river slope 9.1°). Along the Lampenisu

River profile, the Matano Fault, a highly segmented, sinistral strike-slip fault with an extensional component (Watkinson and Hall 2016), creates an elevation offset of about 50 m over a distance of 400 m (average river slope 7.1°), which is also clearly visible in an abrupt change of slope angle in the northern part of the Lampenisu River catchment (Fig. 2). Rivers to the south and northwest have well-developed river profiles. The three major rivers, the Mahalona (north), Loeha (east), Timampu (northwest), and the southernmost rivers, have wide alluvial plains in their lower course. Observations during fieldwork in 2015 indicated that the rivers on these alluvial plains presently cut into fluvial gravel deposits and have wide stream channels with exposed gravel bars along both sides of the active channel.

Laterites

The six laterite profiles investigated (Fig. 3, ESM Fig. S2) varied in thickness between 2 and 6 m and show a clear colour zonation with the uppermost horizon characterised by dark red material (approximately 0.2-1 m thick, 6 samples). Going deeper, this grades into a lighter red colour (0-1 m thick, 5 samples), followed by a yellow intermediate zone (1-2 m thick, 7 samples), then a green-grey-coloured saprolite zone (0.5-3 m thick, 5 samples) just above the unweathered parent rock. The colour zonation is very clearly reflected in elemental gradients, which are similar in soil profiles over varying degrees of bedrock serpentinisation (Fig. 3, ESM Fig. S2). In the laterites, Al, Fe, Ti, K, Cr, Zr, Zn, and Mn are enriched relative to the saprolite and bedrock, peaking in the red rather than the uppermost dark red zone (Fig. 3

351 and ESM Fig. S2). In contrast, Mg and Ca have the highest concentrations in
352 the saprolite and bedrock, and decrease markedly upwards in the laterite (Fig.
353 3 and ESM Fig. S2). Nickel concentrations peak in the saprolite zone with an
354 average concentration of 1.5 ±1.1%. Laterite profiles 1, 3, and 4 are located
355 on slopes and coarse pebbles were visible in the dark red matrix of the
356 uppermost zone, but the pebbles were not included in the samples used for
357 analysis. Average concentrations of Al ranged from 4.3 ±1.2% in the
358 uppermost dark red horizon to 0.9 ±0.9% in the bedrock. Likewise, Fe (dark
359 red zone: 32.8 ±15.8%; bedrock: 5.8 ±0.3%) and Ti (dark red zone: 0.1
360 ±0.06%; bedrock: 0.03 ±0.05%) were concentrated in the laterite relative to
361 unweathered bedrock. Mg concentrations increased from 6.8 ±6.5% in the
362 uppermost horizon to 39.3 ±6.3% in the bedrock. The CIA shows strongly
363 increasing values from bedrock (mean 33.6 ±15.3) to the overlying laterite
364 (mean 94.0 ±9.1).
365
366 Bulk XRD and thin section analyses show that unserpentinised rocks
367 consist of olivine (> 60%), clino- and orthopyroxenes (diopside and enstatite,
368 10-25%), and small amounts (< 5%) of accessory minerals such as magnetite,
369 illmenite, amphiboles, and goethite. Parts of the bedrock have undergone
370 secondary serpentinisation close to the surface (ESM Fig. S3a). The main
371 mineral phases in serpentinised samples are chrysotile and antigorite, with
372 small amounts of magnetite and chlorite. In places, initially serpentinised
373 peridotites have undergone a second alteration to form very fine-grained
374 olivine and amphiboles (tremolite). In the weathering crust of the bedrock
375 samples, serpentine and magnetite rinds are observed around disintegrating

olivine grains (ESM Fig. S3c). Small amounts of (clino)pyroxenes and amphiboles remain present in the saprolite and lower laterite zone. Veins in the saprolite and laterite are filled with very fine-grained secondary quartz crystals (ESM Fig. S3b). In the laterite horizons, goethite is the dominant mineral phase (ESM Fig. S4), and smectites are present in the yellow laterite horizon (ESM Fig. S4). FTIR spectroscopy further indicates the presence of kaolinite in the upper laterite horizons, whereas serpentines are more common in the lower laterite and saprolite zone (ESM Fig. S2c).

Geotechnical parameters of the laterites are summarised in ESM Fig. S5. Grain-size distribution curves are classified as *silt with sand* (ML) for sample Lat 8 a+b (profile 4, red and yellow laterite zone), *elastic silt* (MH) for sample Lat 9 b+c (profile 5, red and yellow laterite zone), *silty sand* (SM) for sample Lat 10 b+c and Sap 3 (profile 6, red laterite zone, and profile 2, saprolite zone, respectively), and *elastic silt with sand* (MH) for sample Lat 10 d+e (profile 6, yellow laterite zone). Coarse fractions (> 0.063 mm) of all five samples are dominated by magnetite grains, with occasional quartz and metal oxide concretions. The internal angles of friction (φ) for samples Lat 10 b+c (red laterite horizon) and 10 d+c (yellow laterite horizon) are 43.8° and 26.5°, respectively, with material density of 2.3 and 1.5 g cm^{-3}, respectively. The φ-angles based on classification of grain size distribution curves are 34° in the saprolite zone, 25-28° in the lower (lower red and yellow zone combined), and 33.6° in the upper laterite (dark red and upper red zone combined) horizons. Plasticity indices (I_P) are around 5% in the upper laterite horizon and saprolite zone, and 20-35% in the lower laterite horizon. Water content is 9.8% in the

saprolite zone, between 44.3 and 104.2% in the yellow laterite horizons, and 17.9% in the red laterite horizon.

Lake surface sediments

Lake surface sediments close to the Mahalona River inflow are characterised by high Mg concentrations, whereas Al, Ni, and Fe concentrations are low (Fig. 4 and ESM Fig. S6). This pattern decreases with increasing distance from the river mouth. Similarly, sediments at the southern tip of the lake are depleted in Al and Ti, and enriched in Mg (Fig. 4). In general, coarser-grained samples show a closer resemblance to bedrock samples, whereas the elemental composition of fine-grained samples is more similar to the composition of the laterites (Fig. 4, ESM Fig. S6). The lake surface sediments have a mean CIA of 79.3 ±8.6. Values are lowest close to the inlets of the Mahalona and Loeha Rivers (CIA < 70), and peak in the northeast and south of the lake (CIA > 85; ESM Fig. S6b). Delta sediments of the Loeha River are characterised by low concentrations of Ni, Cr, Co, and Fe and high concentrations of K, Ti, Al, Sb, and Sr (Fig. 4, ESM Fig. S6, and Hasberg et al. 2018). Except for isolated patches close to shore, e.g. close to the Mahalona River inflow, Al, Ni, and Ti concentrations are mostly homogenous across the lake (Fig. 4 and ESM Fig. S6). Ca and Mg concentrations are generally higher in the northern (Ca: 0.72%; Mg: 7.13%) compared to the southern (Ca: 0.45%; Mg: 5.33%) lake basin.

425 The kaolinite-to-serpentine ratio is high in sediments off the Loeha River
426 inflow and in areas without significant riverine runoff, whereas values are
427 lower close to the Mahalona River and at the inflow of the southernmost rivers
428 (Fig. 4e and ESM Fig. S6g). Clay mineralogical analysis shows general
429 agreement between XRD results of the clay fraction (peak height) and bulk
430 MIR-FTIRS measurements (peak area) for kaolinite and serpentine (Pearson
431 correlation r=0.50, and Spearman's rank correlation r=0.69, respectively,
432 $p<0.01$, n=79, ESM Fig. S1), and also between clay XRD results and Al and
433 Mg concentrations in the bulk sediment (Pearson correlation r=0.56, and
434 Spearman's rank correlation r=0.64, respectively, $p<0.01$, n=79, ESM Fig.
435 S1). Bulk XRD analyses show a decrease in serpentines and amphiboles and
436 an increase in quartz content (ESM Fig. S7) with distance from the Mahalona
437 River, indicating that key elements are related to main mineral composition.
438 The smectite-to-illite ratio is generally lower in the southern lake basin,
439 especially around the Loeha River, whereas smectite is enriched relative to
440 illite in the northern basin (ESM Fig. S6h).
441
442 Sediment cores
443
444 Coring location Co1230 is more heavily influenced by hyperpycnal flows and
445 turbidite deposition from the Mahalona Delta compared to coring location
446 TOW9 (Vogel et al. 2015). The fine-grained pelagic sediments of the two
447 cores, however, show very similar trends in their geochemical composition.
448 The Al/Mg ratio is low in the middle to late Holocene (6-4 kyr BP), between 27
449 and 15 kyr BP, and prior to 58 kyr BP (TOW9 only, Fig. 5a). High Al/Mg

values occur at 2 and 13-11 kyr BP, between 41-32 kyr BP, and at 55 kyr BP. Ti concentrations show a similar pattern, which is overlain by an overall decreasing trend from 55 to 15 kyr BP (Fig. 5b, Russell et al. 2014).

Kaolinite and serpentine measured by clay-size MIR-FTIRS (band depth) and clay XRD (peak height) in Co1230 are strongly correlated (Pearson correlation r=0.77, and r=0.73, respectively, $p<0.01$, n=14, ESM Fig. S1), as are clay XRD kaolinite and serpentine with concentrations of bulk Al and Mg (Pearson correlation r=0.71, and r=0.87, respectively, $p<0.01$, n=15, ESM Fig. S1). Core TOW9 shows coherent trends in clay XRD kaolinite and serpentine and concentrations of Al and Mg over the past 60 kyr (Fig. 5a and c), but clay XRD and geochemical concentrations were not determined on the same sediment horizons, precluding analysis of correlation. The kaolinite-to-serpentine ratio is generally higher between 55 and 27 kyr BP compared to 27-0 kyr BP and prior to 58 kyr BP. For the past ~40 kyr, a similar pattern appears for kaolinite and serpentine, determined by near-infrared spectroscopy on other sediment cores from Towuti's northern basin (Goudge et al. 2017).

Discussion

Weathering and erosion processes in Lake Towuti's catchment

The laterite profiles around Lake Towuti closely follow a geochemical and mineralogical zonation characteristic of well-developed tropical laterites (Colin

et al. 1990; Brand et al. 1998; Marsh et al. 2013). We did not observe major differences in laterite zonation and elemental composition between the laterites across varying degrees of bedrock serpentinisation (ESM Fig. S2). Bedrock and laterite mineralogy indicate that olivine weathers readily whereas pyroxene remains present in the saprolite zone and lower laterite horizons. Veins in the saprolite and laterite consist mainly of secondary quartz (ESM Fig. S3) and may thus serve as a quartz source to the lake sediments in the ultramafic part of the lake catchment. Very high goethite concentrations in the upper laterite horizon and steep element concentration gradients through the laterite horizons indicate that most other components have been transformed or leached from the profiles (Golightly and Arancibia 1979; ESM Fig. S4).

Peak elemental concentrations in the red rather than the uppermost dark red zone of laterite profiles from slope positions, e.g. in Fe and Al (Fig. 3, ESM Fig. S2a), suggest surficial reworking by slope processes. Coarse pebbles in the uppermost zone of some profiles support the idea of potential input of less weathered material from upslope positions. Features of slope processes, including slope creep and mass wasting, were clearly visible during fieldwork. Slopes with a steepness above the empirically determined critical angle of friction (25-43°, i.e. areas that exceed the Mohr-Coulomb failure criterion) are found throughout the catchments and suggest that slope processes such as landslides are a prevalent feature in catchments around Lake Towuti and possibly similarly structured tropical catchments. Geotechnical analyses of the laterites around Towuti (ESM Fig. S5) suggest that upper laterite horizons have a larger grain size, lower water uptake

capacity (I_P of ~5%), and are stable at higher slope angles (φ-angle 43.8°) compared to clay-rich lower laterite horizons with water content of up to 100% (I_P of 18-20%) and a low (26.5°) critical angle of internal friction. Our analysis suggests that lower laterite horizons fail more readily compared to upper soil layers and thus function as a slip plane, mobilising the entire soil package when slope failures occur.

Seismicity-induced slope failure has been recognised as an important process in the erosion of tropical landscapes (Thomas 1996), and in Lake Towuti's active tectonic setting, strong earthquakes occur regularly (Jones et al. 2014). Recently, a shallow-focus M_W 6.1 earthquake occurred in 2011 at the shore of Lake Matano, with a potential surface rupture length of 39 km (Watkinson and Hall 2016). Detailed tectonic studies of the area are still lacking, but geomorphologic evidence and fault kinematics analyses suggest rapid slip rates along the Matano fault and activity throughout the Quaternary (Bellier et al. 2006). Our analysis therefore suggests seismically triggered slope failures are important to erosion and sediment supply in tectonically active landscapes. In such environments, fault activity and seismic events enhance the mobilisation of the entire soil package, despite dense vegetation cover, and facilitate erosion of fine-grained soil material below the compacted upper laterite crust. In addition, slope processes also contribute directly to sedimentation in near-shore areas. Especially in the W and NE of the lake, steep slopes are located close to the lakeshore, such that mass movement material can directly reach the lake without intermediate fluvial transport and sorting of the material. During fieldwork in 2015, several mass movement

deposits, which directly reach the lake shore, were observed. There is, however, no indication that such material directly reaches the coring sites in the deep northern lake basin.

Tectonics and lithologic changes also strongly affect the river catchments around Lake Towuti (Figs. 2 and 3). Steep hillslopes (> 26°) along the Mahalona River and its tributaries north of the Matano Fault trace, in contrast to slope angles of mostly less than 5° located south of the fault (Fig. 2), suggest a strong influence of tectonics on sediment mobilisation and composition. Tectonic uplift and earthquake-triggering of slope failures in this catchment provide a constant flux of sediment to the river system, and ultimately, to the lake. Gravel deposits that accumulated in former riverbeds of the alluvial plain, observed during fieldwork, point to a sizeable contribution of remobilized sediments in the overall load that enters the lake. To the east of Lake Towuti, bedrock abrasion at the river knickpoint of the Loeha River, in combination with tectonic disturbance along a fault running parallel to the eastern lake shore (Watkinson and Hall 2016), likely explains the strong geochemical difference of the Loeha compared to the other rivers (ESM Fig. S8). As such, relatively small river catchments that are strongly influenced by tectonic disturbance can exert a strong influence on the geochemical composition of sediments deposited in the lake. Profiles of the smaller rivers to the northwest and south show no signs of recent tectonic activity, which results in a relatively low erosive capacity compared to the Mahalona and Loeha Rivers and thus a smaller influence on sediment composition at the sink.

550

551 The influence of erosional processes on lake sedimentation

552

553 The lake surface sediment geochemistry provides detailed information on the
554 spatial variations in erosional processes and sediment composition in Lake
555 Towuti. In areas of the lake where catchments are small and steep and valley
556 incision is minimal, e.g. in the NE and SW, the elemental composition of the
557 surface sediment closely resembles the laterite horizons. In these areas,
558 slopes above the critical angle of friction are located close to the lake and
559 mass movement processes may provide an important contribution to
560 sedimentation. This is supported by high CIA values indicating weathered
561 material across the western and northeastern parts of the lake compared to
562 poorly weathered material delivered by the Mahalona and Loeha Rivers (ESM
563 Fig. S6b). Clay mineralogy analysis also shows a high kaolinite-to-serpentine
564 ratio across the southern lake basin and close to the western lakeshore,
565 where river inflow is small (Fig. 4e). In these areas, laterite material may also
566 be mobilised and transferred into the lake by shore erosion.

567

568 Geochemistry and mineralogy of the lake sediments (Fig. 4) close to
569 major rivers, e.g. the Mahalona, show that these rivers cut deeply through the
570 laterite soils, transporting fresh or poorly weathered material that is derived
571 from the bedrock and saprolite zone (ESM Fig. S8; Goudge et al. 2017). This
572 signal is also amplified by hydrodynamic sorting in the river deltas (ESM Fig.
573 S6; data described in detail by Hasberg et al. 2018). In addition to providing a
574 more complete picture of the spatial extent of fluvial influence in the northern

basin compared to previous studies, our results also confirm the finding by Costa et al. (2015), Vogel et al. (2015), and Goudge et al. (2017) that the Mahalona River exerts a dominant control on the present-day sediment composition of Towuti's northern basin. Our data further indicate that the mobilisation of fluvial deposits from the alluvial plains of the major rivers likely plays a role in lake sedimentation close to the river mouths.

Al/Mg as a proxy for lake level changes

The spatial patterns of chemically inert elements in the lake (e.g. Al, Mg, K, and Ti) show that today's sediment composition in the deep northern lake basin is a mixture of bedrock-derived sediments from the Mahalona River, sediments from the Loeha River, and laterite-derived input (ESM Fig. S8). In the catchment, Al, K, and Ti are enriched in the laterite horizons, whereas Mg is a characteristic element in the bedrock. Because K and Ti concentrations are relatively low (< 1% in the lake sediments; Fig. 4), the ratio of Al and Mg was chosen to represent the relative contribution of bedrock and laterite erosion in Towuti's catchment. The Al/Mg patterns (Fig. 4f) correspond to gradients in mineralogy, namely in the abundance of kaolinite and serpentine in laterite and bedrock (as expressed in the kaolinite-to-serpentine ratio). Sediments sourced from the Loeha River are characterised by higher K concentrations relative to the rivers draining ultramafic catchments (ESM Fig. S8). The chemical composition of lake sediments and the sediment cores suggests that the Loeha River has a small (< 10%) but detectable influence on sediment composition at the coring site (ESM Fig. S8). The Loeha River

600 currently drains into the southern basin, but Costa et al. (2015) suggested that
601 sediment from the Loeha reaches the location of core TOW9. The Al/Mg ratio
602 at the locations of TOW9 (0.56) and Co1230 (0.87) also indicates sources
603 other than the Mahalona River (Al/Mg of 0.15 and 0.21 in bedload and
604 suspended load, respectively; Goudge et al. 2017), e.g. input from laterite
605 soils (Al/Mg between 0.83 and 2.14, Fig. 3) and the Loeha River (Al/Mg=2.62;
606 Costa et al. 2015). Fine-grained Mahalona River sediments (Al/Mg of 0.32
607 and 0.37 in bedload and suspended load < 32 µm, respectively; Goudge et al.
608 2017) and smaller rivers entering the northern basin (Al/Mg between 0.22 and
609 0.28; Costa et al. 2015; ESM Fig. S8; no data available for the Timampu
610 River) cannot account for such high values. Therefore, the Al/Mg ratio and the
611 relation between Al-Mg-K provide information about the importance of the
612 Mahalona relative to the Loeha River and laterite-derived sediments (ESM
613 Fig. S8).
614
615 Although bedrock geology, tectonic processes, and erosion in the
616 catchment regulate the general composition of sediments in the lake, this
617 composition is modified by changes in regional hydroclimate and lake level
618 fluctuations. Decreased lake levels lead to a lower hydrologic base level and
619 increased hydrologic gradients, which cause deeper incision. This favours
620 bedrock erosion relative to surficial laterite erosion, and thus a lower Al/Mg
621 ratio of the Mahalona River during lake level low stands. Remobilisation of
622 bedrock-derived material in the alluvial river plains during lake-level low
623 stands favours the deposition of Mg-rich material in the deeper lake basins.
624 Furthermore, following the interpretation of Vogel et al. (2015), a lower lake

level decreases the distance between the shoreline and coring sites, causing a stronger influence of riverine suspended load and an increase in grain size at the coring locations. Because large grain sizes are enriched in Mg relative to Al (Goudge et al. 2017), this effect lowers Al/Mg during dry periods. In addition, runoff is reduced, which decreases discharge volume and long-distance sediment transport capacity of the rivers. This likely reduces the influence of the Loeha River relative to the Mahalona River, which is located much closer to the coring site. Hence, we expect a lower Al/Mg ratio in the northern lake basin during drier climate conditions. In contrast, during lake-level high stands, lower hydrologic gradients favour a higher proportional erosion of laterite soils compared to bedrock incision, and a change from erosion to accumulation in the alluvial plains around the lake. The distance between shoreline and coring sites increases, which decreases grain size, whereas higher river discharge may increase long-distance transport capacity of the rivers, increasing the influence of the Loeha River at the coring site. These factors all increase the Al/Mg in the lake sediments during wet phases. Therefore, a high Al/Mg ratio indicates wet phases in the regional climate.

Disentangling the relative influences of tectonics and climate on lake sediment composition over time can be challenging. If fault activity in the whole lake catchment changes, sedimentation rates in the lake should change accordingly. This is not apparent in our sediment records, which span the past 60,000 years. If fault activity was enhanced along the Matano Fault, both river incision and soil erosion from steepening slopes in the river catchment should increase. If both effects were equally strong over millennial time scales,

650 tectonic activity along the Matano Fault would not change the Al/Mg ratio in
651 the lake significantly. In contrast, if the Loeha catchment is more strongly
652 influenced by tectonics, K deposition at the coring sites should increase
653 relative to Mg. This is more difficult to disentangle in the record, but an
654 increase in kaolinite from the laterites, coinciding with an increase in K from
655 the Loeha and a decrease in Mg from the Mahalona, would generally point
656 towards climate (i.e. higher lake levels) rather than tectonics as the driving
657 factor for the observed changes.
658
659 Lake Towuti's palaeoclimate record
660
661 In the past 60 kyr, Al/Mg, K, and kaolinite show similar trends in the record
662 (Fig. 5), suggesting a dominant influence of climate processes on pelagic
663 sedimentation in the northern basin. Changes in the past 30 kyr are seen at
664 both coring sites, TOW9 and Co1230 (excluding event layers; Fig. 5a and b),
665 emphasizing the homogeneity of pelagic sedimentation in the northern basin.
666 In the past 60 kyr, the Al/Mg ratio shows lowest values in the mid-Holocene
667 (6-4 kyr BP), in MIS2, and around 58 kyr BP (Fig. 5a). The latter two intervals
668 correspond to glacial periods with substantial extents of northern hemisphere
669 ice sheets. Based on data from the modern lake, our proxy record suggests
670 that lake level was lower and climate conditions were drier during these
671 periods compared to today. Accordingly, high Al/Mg values in the late
672 Holocene, at the transition from the last glacial period, and during MIS3,
673 indicate lake level highstands and a wet climate in Central Sulawesi. Our
674 findings are in line with earlier studies from Lake Towuti (Russell et al. 2014;

675 Costa et al. 2015; Vogel et al. 2015; Goudge et al. 2017), other studies from
676 Sulawesi (Dam et al. 2001; Hope 2001; Dubois et al. 2014; Wicaksono et al.
677 2015, 2017), and from the Indo-Pacific Warm Pool region (De Deckker et al.
678 2002; Reeves et al. 2013), indicating a dry last glacial period. Vegetation
679 around Lake Towuti, which is sensitive to climate rather than tectonics, also
680 shows regional drying during MIS2 and wet conditions during MIS1 and MIS3
681 (Russell et al. 2014). These results suggest that climate was the dominant
682 factor that shaped sedimentation in Lake Towuti over the last 60,000 years.
683
684 Interestingly, the Lake Towuti record indicates a pronounced dry period
685 during the mid-Holocene (6-4 kyr BP) with minima in both the Al/Mg and
686 kaolinite-to-serpentine ratios. This was described previously in a record from
687 Lake Towuti that covered the last 45,000 years, and together with smaller
688 variations during MIS2, was attributed to an 11-kyr, half-precessional signal
689 (Goudge et al. 2017). Our longer, 60,000-year record suggests that during
690 MIS3, this potential 11-kyr cylicity is less pronounced or absent. This may be
691 a consequence of a more dominant influence of the strong tilt of Earth's axis
692 on northern hemisphere ice sheet extent during MIS3 (Van Meerbeeck et al.
693 2009; Svendsen et al. 2004; Helmens et al. 2007) and/or the influence of
694 millennial-scale events triggered in the North Atlantic that are not resolved in
695 our data time series (Dansgaard et al. 1993). Alternatively, other mechanisms
696 may be responsible for the pronounced dry period during the mid-Holocene,
697 which would require further investigation.
698
699 **Conclusions**

Source-to-sink analysis of the geochemistry and clay mineralogy of Lake Towuti provided insights into the modern erosional processes and sediment composition in a tropical lake catchment characterized by ultramafic bedrock composition, lateritic soils, and active tectonics. Mass movement processes, tectonic disturbance of river profiles, and climate-induced remobilisation of fluvial deposits strongly influenced sedimentation at this site. Lower soil horizons can function as a slide plane during mass movement events, mobilising the soil package and contributing substantially to erosion in the steeper parts of this tropical catchment. In the northeastern and western lake catchment such mass movement events may supply material directly to the lake, whereas larger, tectonically disturbed rivers mainly erode and transport bedrock-derived material to the lake. Our analysis of the river profiles, along with spatially explicit analysis of surface sediment composition, added an additional, more process-based understanding of the contribution of tectonic disturbance to the sediment load delivered to the sink. In general, fault movement greatly influences the amount and dispersion of sediment delivered to the sink by disturbed, relative to less-disturbed, river systems.

Although tectonic processes and erosion in the catchment influence the general composition of the lake sediments, this composition is modified by changes in the regional hydroclimate over glacial-interglacial timescales. Based on the understanding of today's lake system, we identified the Al/Mg ratio as a proxy for lake level changes, which provide the dominant sedimentary signal for regional hydroclimate changes. Characterising and

understanding the functioning of the modern lake system is crucial for the development and interpretation of sediment proxies, especially in geochemically exceptional lake systems such as Towuti. The complexity of processes described for this tropical lake catchment, in combination with the sampling and analytical approach applied, may help to inform future studies that aim to acquire information on landscape evolution in similar settings.

Acknowledgements

The Towuti Drilling Project was partially supported by grants from the International Continental Scientific Drilling Program, the US National Science Foundation, the German Research Foundation, the Swiss National Science Foundation (20FI21_153054/1 and 200021_153053/1), Brown University, Genome British Columbia, and the Ministry of Research, Technology, and Higher Education (RISTEK). PT Vale Indonesia, the US Continental Drilling Coordination Office, the GeoForschungszentrum Potsdam and DOSECC Exploration Services are acknowledged for logistical assistance to the project. We further thank Franziska Nyffenegger for support with the geotechnical analysis, Urs Eggenberger and Christine Lemp for help with the clay and bulk XRD analysis, Elias Kempf for assistance with thin section analysis, as well as Pierre Valla and Romain Delunel for fruitful discussions regarding the geomorphic aspects of the study. This research was carried out with permission from the Ministry of Research and Techonology (RISTEK), the Ministry of Trade of the government of Indonesia, and the Natural Resources Conservation Center (BKSDA) and Government of Luwu Timur of Sulawesi.

We also wish to thank two anonymous reviewers and the editors for their helpful comments and suggestions, which improved our manuscript.

754 ## References

755

756 Adunoye GO (2014) Fines Content and Angle of Internal Friction of a Lateritic
757 Soil: An Experimental Study. Am J Engin Res 3: 16-21

758 Bellier O, Sébrier M, Seward D, Beaudouin T, Villeneuve M, Putranto E
759 (2006) Fission track and fault kinematics analyses for new insight into the
760 Late Cenozoic tectonic regime changes in West-Central Sulawesi (Indonesia).
761 Tectonophysics, 413: 201-220. DOI: 10.1016/j.tecto.2005.10.036

762 Brand NW, Butt CRM, Elias M (1998) Nickel laterites: classification and
763 features. J Aust Geol Geophys 17: 81-88

764 Casagrande L (1932) Research of Atterberg Limits of Soils. Public Roads 13:
765 121-136

766 Chester R, Elderfield H, (1973) An infrared study of clay minerals, 2. The
767 identification of kaolinite-group clays in deep-sea sediments. Chem Geol 12:
768 281-288

769 Chukanov NV (2014) Infrared Spectra of Mineral Species. Springer, Dordrecht

770 Colin F, Nahon D, Trescases JJ, Melfi AJ (1990) Lateritic Weathering of
771 Pyroxenites at Niquelandia, Goias, Brazil: The Supergene Behavior of Nickel.
772 Econ Geol 85: 1010-1023

773 Costa KM, Russell JM, Vogel H, Bijaksana S (2015) Hydrological connectivity
774 and mixing of Lake Towuti, Indonesia in response to paleoclimatic changes
775 over the last 60,000 years. Palaeogeogr Palaeoclimatol Palaeoecol 417: 467-
776 475. DOI: 10.1016/j.palaeo.2014.10.009

777 Crowe SA, Jones C, Katsev S, Magen C, O'Neill AH, Sturm A, Canfield DE,
778 Haffner GD, Mucci A, Sundby B, Fowle DA (2008) Photoferrotrophs thrive in
779 an Archean Ocean analogue. Proc Natl Acad Sci USA 105: 15938-43. DOI:
780 10.1073/pnas.0805313105

781 Dansgaard W, Johnsen SJ, Clausen HB, Dahl-Jensen D, Gundestrup NS,
782 Hammer CU, Hvidberg CS, Steffensen JP, Sveinbjörnsdottir AE, Jouzel J,
783 Bond G (1993) Evidence for general instability of past climate from a 250-kyr
784 ice-core record. Nature 364: 218-220

785 Dam RAC, Fluin J, Suparan P, van der Kaars S (2001) Palaeoenvironmental
786 developments in the Lake Tondano area (N. Sulawesi, Indonesia) since
787 33,000 yr BP. Palaeogeogr Palaeoclimatol Palaeoecol 171: 147-183

788 De Deckker P, Tapper NJ, van der Kaars S (2002) The status of the Indo-
789 Pacific Warm Pool and adjacent land at the Last Glacial Maximum. Glob
790 Planet Chang 35: 25-35

791 DIN 18137-1. German Industrial Norm (2010) Baugrund, Untersuchung von
792 Bodenproben. Bestimmung der Scherfestigkeit, Teil 1: Begriffe und
793 grundsätzliche Versuchsbedingungen [Soil, investigation and testing -

794 Determination of shear strength - Part 1: Concepts and general testing
795 conditions]

796 DIN 18137-3. German Industrial Norm (2002) Baugrund, Untersuchung von
797 Bodenproben. Bestimmung der Scherfestigkeit, Teil 3: Direkter Scherversuch
798 [Soil, investigation and testing - Determination of shear strength - Part 3:
799 Direct shearing test]

800 Dubois N, Oppo DW, Galy VV, Mohtadi M, van der Kaars S, Tierney JE,
801 Rosenthal Y, Eglinton TI, Lückge A, Linsley BK (2014) Indonesian vegetation
802 response to changes in rainfall seasonality over the past 25,000 years. Nat
803 Geosci 7: 513–517. DOI: 10.1038/ngeo2182

804 Farmer VC (1974) The infrared spectra of minerals. Mineralogical society
805 monograph 4. Adlard and Son, Dorking, UK.

806 Golightly JP, Arancibia ON (1979) The chemical composition and infrared
807 spectrum of nickel- and iron-substituted serpentine from a nickeliferous
808 laterite profile, Soroako, Indonesia. Can Mineral 17: 719-728

809 Goudge TA, Russell JM, Mustard JF, Head JW, Bijaksana S (2017) A 40,000
810 yr record of clay mineralogy at Lake Towuti, Indonesia: Paleoclimate
811 reconstruction from reflectance spectroscopy and perspectives on paleolakes
812 on Mars. Bull Geol Soc Am 129: 806-819. DOI: 10.1130/B31569.1

813 Haffner GD, Hehanussa PE, Hartoto D (2001) The biology and physical
814 processes of large lakes of Indonesia: Lakes Matano and Towuti. In: Munawar

M, Hecky RE (eds) The Great Lakes of the World (GLOW). Michigan State University Press, 183-192

Hasberg AKM, Melles M, Wennrich V, Just J, Held P, Morlock MA, Vogel H, Russell JM, Bijaksana S, Opitz S (2018) Modern sedimentation processes in Lake Towuti, Indonesia, revealed by the composition of surface sediments. Sedimentology. DOI: 10.1111/sed.12503

Helmens KF, Bos JAA, Engels S, Van Meerbeeck CJ, Bohncke SJP, Renssen H, Heiri O, Brooks SJ, Seppä H, Birks HJB, Wohlfarth B (2007) Present-day temperatures in northern Scandinavia during the last glaciation. Geology 35: 987-990. DOI: 10.1130/G23995S1

Hope G (2001) Environmental change in the Late Pleistocene and later Holocene at Wanda site, Soroako, South Sulawesi, Indonesia. Palaeogeogr Palaeoclimatol Palaeoecol 171: 129-145

Jones ES, Hayes GP, Bernardino M, Dannemann FK, Furlong KP, Benz HM, Villaseñor A (2014) Seismicity of the Earth 1900–2012, Java and vicinity. U.S. Geological Survey Open-File Report 2010–1083-N, 1 sheet, scale 1:5,000,000, DOI: 10.3133/ofr20101083N

Kadarusman A, Miyashita S, Maruyama S, Parkinson CD, Ishikawa A (2004) Petrology, geochemistry and paleogeographic reconstruction of the East Sulawesi Ophiolite, Indonesia. Tectonophysics. 392: 55-83. DOI: 10.1016/j.tecto.2004.04.008

836 Konecky B, Russell JM, Bijaksana S (2016) Glacial aridity in central Indonesia
837 coeval with intensified monsoon circulation. Earth Planet Sci Lett 437: 15-24.
838 DOI: 10.1016/j.epsl.2015.12.037

839 Madejová J (2003) FTIR techniques in clay mineral studies. Vib Spectrosc 31:
840 1-10

841 Marsh E, Anderson E, Gray F (2013) Nickel-Cobalt Laterites - A Deposit
842 Model. In: Mineral Deposit Models of Resource Assessment. U.S. Geological
843 Survey, Reston, USA

844 Nesbitt HW, Young GM (1982) Early Proterozoic climates and plate motions
845 inferred from major element chemistry of lutites. Nature 299: 715-717

846 Ogunsanwo O (1988) Basic Geotechnical Properties, Chemistry and
847 Mineralogy of some Laterite Soils from S.W. Nigeria. Bull Int Assoc Engin
848 Geol: 131-135

849 Omotoso OA, Ojo OJ, Adetolaju ET (2012) Engineering Properties of Lateritic
850 Soils around Dall Quarry in Sango Area, Ilorin, Nigeria. Earth Sci Res 1: 71-
851 81. DOI: 10.5539/esr.v1n2p71

852 R Development Core Team (2008) R: A language and environment for
853 statistical computing. R Foundation for Statistical Computing. Available at:
854 www.r-project.org (last accessed Feb 13 2017)

855 Reeves JM, Bostock HC, Ayliffe LK, Barrows TT, De Deckker P, Devriendt
856 LS, Dunbar GB, Drysdale RN, Fitzsimmons KE, Gagan MK, Griffiths ML,

857 Haberle SG, Jansen JD, Krause C, Lewis S, McGregor HV, Mooney SD,
858 Moss P, Nanson GC, Purcell A, van der Kaars S (2013) Palaeoenvironmental
859 change in tropical Australasia over the last 30,000 years – a synthesis by the
860 OZ-INTIMATE group. Quat Sci Rev 74: 97-114. DOI:
861 10.1016/j.quascirev.2012.11.027

862 Robinson GW (1922) A new method for the mechanical analysis of soils and
863 other dispersions. J Agric Sci 12: 306-321

864 Russell JM, Vogel H, Konecky B, Bijaksana S, Huang Y, Melles M, Wattrus N,
865 Costa KM, King JW (2014) Glacial forcing of central Indonesian hydroclimate
866 since 60,000 y BP. PNAS 111: 5100-5105. DOI: 10.1073/pnas.1402373111

867 Russell JM, Bijaksana S, Vogel H, Melles M, Kallmeyer J, Ariztegui D, Crowe
868 S, Fajar S, Hafidz A, Haffner D, Hasberg A, Ivory S, Kelly C, King J, Kirana K,
869 Morlock M, Noren A, O'Grady R, Ordonez L, Stevenson J, von Rintelen T,
870 Vuillemin A, Watkinson I, Wattrus N, Wicaksono S, Wonik T, Bauer K, Deino
871 A, Friese A, Henny C, Imran, Marwoto R, Ngkoimani LO, Nomosatryo S,
872 Safiuddin LO, Simister R, Tamuntuan G (2016) The Towuti Drilling Project:
873 paleoenvironments, biological evolution, and geomicrobiology of a tropical
874 Pacific lake. Sci Drill 21: 29-40. DOI: 10.5194/sd-21-29-2016

875 Sagapoa CV, Imai A, Watanabe K (2011) Laterization Process of Ultramafic
876 Rocks in Siruka, Solomon Islands. J Nov Carb Resourc Sci 3: 32-39

877 SN 670 010. Swiss Norm. Geotechnische Erkundung und Untersuchung -
878 Geotechnische Kenngrössen [G*eotechnical exploration and analysis -*
879 *Geotechnical parameters*]. Edition 2011-08

880 SN 670 816a. Swiss Norm. Mineralische Baustoffe, Schlämmanalyse nach
881 der Aräometermethode [Minerogenic material – Sieving analysis by
882 aerometric method]

883 SN 670 902-1 (EN 933-1). Swiss Norm. Prüfverfahren für geometrische
884 Eigenschaften von Gesteinskörnungen. Teil 1: Bestimmung der
885 Korngrössenverteilung - Siebverfahren [Testing geometric properties of
886 grains, Part 1: Grain-size distribution – Sieving]. Edition 2013-03

887 SN 670 345b. Swiss Norm. Böden - Konsistenzgrenzen [Soils – Plasticity
888 Index]

889 Svendsen JI, Alexanderson H. Astakhov VI, Demidov I, Dowdeswell JA,
890 Funder S, Gataullin V, Henriksen M, Hjort C, Houmark-Nielsen M, Hubberten
891 HW, Ingólfsson Ó, Jakobsson M, Kjær KH, Larsen E, Lokrantz H, Lunkka JP,
892 Lysså A, Mangerud J, Matiouchkov A, Murray A, Möller P, Niessen F,
893 Nikolskaya O, Polyak L, Saarnisto M, Siegert C, Siegert MJ, Spielhagen RF,
894 Stein R (2004) Late Quaternary ice sheet history of northern Eurasia. Quat
895 Sci Rev 23: 1229-1271. DOI: 10.1016/j.quascirev.2003.12.008

896 Thomas MF (1996) Geomorphology in the tropics. Wiley, Chichester, UK

U.S. Geological Survey (2017) Mineral Commodity Summaries 2017. U.S. Geological Survey, Reston, USA. DOI: 10.3133/70180197

Van Meerbeeck CJ, Renssen H, Roche DM (2009) How did Marine Isotope Stage 3 and Last Glacial Maximum climates differ? - Perspectives from equilibrium simulations. Clim Past 5: 33-51

Vogel H, Russell JM, Cahyarini SY, Bijaksana S, Wattrus N, Rethemeyer J, Melles M (2015) Depositional modes and lake-level variability at Lake Towuti, Indonesia, during the past ~29 kyr BP. J Paleolimnol 54: 359-377. DOI: 10.1007/s10933-015-9857-z

Von Rintelen T, Von Rintelen K, Glaubrecht M, Schubart CD, Herder F (2012) Aquatic biodiversity hotspots in Wallacea: the species flocks in the ancient lakes of Sulawesi, Indonesia. In: Gower DJ, Johnson K, Richardson J, Rosen B, Rüber L, Williams S (eds). Biotic Evolution and Environmental Change in Southeast Asia, Cambridge University Press, Cambridge, UK, pp 291-315

Watkinson IM, Hall R (2016) Fault systems of the eastern Indonesian triple junction: evaluation of Quaternary activity and implications for seismic hazards. In Cummins PR, Meilano I (eds.). Geohazards in Indonesia: Earth Science for Disaster Risk Reduction. Geological Society, London, UK, Special Publications: 441, pp 71-120

Weber AK, Russell JM, Goudge TA, Salvatore MR, Mustard JF, Bijaksana S (2015) Characterizing clay mineralogy in Lake Towuti, Indonesia, with

reflectance spectroscopy. J Paleolimnol 54: 253-261. DOI: 10.1007/s10933-015-9844-4

Whipple KX, Kirby E, Brocklehurst SH (1999) Geomorphic limits to climate-induced increases in topographic relief. Nature 401: 39-43. DOI: 10.1038/43375

Wicaksono SA, Russell JM, Bijaksana S (2015) Compound-specific carbon isotope records of vegetation and hydrologic change in central Sulawesi, Indonesia, since 53,000 yr BP. Palaeogeogr Palaeoclimatol Palaeoecol 430: 47-56. DOI: 10.1016/j.palaeo.2015.04.016

Wicaksono SA, Russell JM, Holbourn A, Kuhnt W (2017) Hydrological and vegetation shifts in the Wallacean region of central Indonesia since the Last Glacial Maximum. Quat Sci Rev 157: 152-163. DOI: 10.1016/j.quascirev.2016.12.006

Widdowson M (2007) Laterite and Ferricrete. In: Nash DJ, McLaren SJ (eds). Geochemical Sediments and Landscapes. Blackwell Publishing, Malden, USA, pp. 46-94

ESM Table S1

Geomorphological characteristics for all major rivers and their respective catchments around Lake Towuti. Values and catchment boundaries are based on DEM analysis. River slope values are averaged over a horizontal distance of 600 m

River	Catchment size [km^2]	River length [km]	Elevation difference [m]	Mean slope catchment [°]	Max. slope catchment [°]	Mean slope river [°]	Max. slope river [°]	sampled
1 (Timampu)	141	18	540	13.1	63	1.6	8.7	no
2 (Mahalona)	293	43	620	14.5	64	0.8	4.9	yes
3 (unknown)	27	12	600	13.2	54	4	7.8	no
4 (LemoLemo)	52	13	695	16.5	67	3	12.8	yes
5 (Tomerakah)	58	12	400	15.2	55	1.8	6.2	yes
6 (Loeha)	84	21	680	15.5	62	1.9	16.2	yes
7 (Lelebiu)	9	5	150	13.2	41	-	-	yes
8 (unknown)	45	10	310	14.5	50	1.7	7.9	no
9 (Tokolalo)	40	14	510	15.2	51	1.9	10.5	yes
10 (Lantibu)	20	9	690	14.8	47	-	-	yes
11 (Lengke)	49	10	510	12.4	45	2.5	17.5	yes
No permanent river	157	-	-	-	-	-	-	yes

Malili Lakes	Lake surface area [km^2]	Catchment size [km^2] (without lake)
Lake Matano	160.5	295
Lake Mahalona	22.2	205
Lake Towuti	559.9	1144

ESM Table S2

Element concentration for the six individual laterite profiles presented in this study. Concentrations were determined by a) ICP-MS and b) WD-XRF. Lower detection limits for ICP-MS measurements are indicated in row 3. *) Sample SAP2 was taken from a secondary quartz vein

a

Sample ID	Profile No.	Profile depth [m]	Laterite horizon	Al	Ca	Cr	Cu	Fe	K	Na	Ni	P	Mg	Mn	Ti	Zn	Zr
				%	%	ppm	ppm	%	%	%	ppm	%	%	ppm	%	ppm	ppm
				0.01	0.01	1	0.1	0.01	0.01	0.001	0.1	0.001	0.01	1	0.001	1	0.1
LAT2	1	0.40	dark red horizon	3.60	0.22	> 10000	83.5	38.40	< 0.01	0.004	9420.0	0.010	7.09	6450	0.061	310	13.0
LAT3	1	1.00	yellow horizon	3.28	< 0.01	> 10000	88.1	38.10	< 0.01	0.004	9560.0	0.004	1.05	6470	0.047	332	7.9
LAT4	1	1.50	yellow horizon	5.24	< 0.01	> 10000	87.2	46.40	< 0.01	0.002	9780.0	0.008	0.86	3070	0.095	346	24.8
LAT5	1	2.20	yellow horizon	2.60	0.02	9650	66.8	24.30	< 0.01	0.007	7560.0	0.003	1.34	5360	0.029	190	3.1
SAP1	1	4.00	saprolite	0.34	0.36	3650	6.9	6.33	< 0.01	0.009	> 10000	0.001	20.10	1020	0.005	64	0.9
SAP2*	1	4.00	saprolite	0.16	0.05	1010	5.6	2.12	0.01	0.006	4420.0	0.001	2.81	406	0.002	34	0.7
BED8 weathered	1	8.00	bedrock	0.71	1.12	2280	16.5	6.23	< 0.01	0.006	3640.0	0.001	29.70	925	0.007	55	0.9
BED8 unweathered	1	8.00	bedrock	0.59	1.22	2430	21.2	6.24	< 0.01	0.005	2290.0	< 0.001	> 30.0	1000	0.007	53	1.0
LAT6a	2	0.10	dark red horizon	3.41	< 0.01	> 10000	84.4	47.30	< 0.01	0.002	> 10000	0.010	0.74	7070	0.137	466	10.7
LAT6b	2	2.00	red horizon	2.93	0.02	> 10000	84.9	48.60	< 0.01	0.002	> 10000	0.007	1.13	8600	0.108	440	6.6
SAP3 weathered	2	2.50	saprolite	2.02	2.41	3190	35.9	6.26	< 0.01	0.167	8460.0	0.002	21.70	820	0.055	240	2.8
SAP3 unweathered	2	2.50	saprolite	1.61	2.38	2030	15.6	5.83	< 0.01	0.136	3690.0	0.002	26.90	954	0.045	58	1.7
BED9	2	3.50	bedrock	0.11	0.02	2060	3.3	5.51	< 0.01	0.005	2310.0	0.001	24.00	710	0.003	59	0.8
LAT7a	3	0.30	dark red horizon	2.87	0.67	6280	45.2	12.30	0.06	0.094	> 10000	0.004	12.80	1970	0.106	120	10.8
LAT7b	3	1.00	yellow horizon	2.17	0.80	7490	34.3	14.90	0.04	0.027	> 10000	0.004	10.80	2670	0.047	123	4.2
BED12	3	8.00	bedrock	0.73	0.69	3560	29.1	5.40	< 0.01	0.012	2000.0	< 0.001	29.20	913	0.008	54	1.1
LAT8c	4	0.05	dark red horizon	5.91	0.66	> 10000	63.3	14.90	0.01	0.051	4490.0	0.018	7.30	6650	0.220	253	13.7
LAT8a	4	0.40	red horizon	4.36	0.31	6700	71.7	33.90	< 0.01	0.033	4810.0	0.005	4.75	3480	0.148	175	13.0
LAT8b	4	1.20	yellow horizon	4.84	0.25	6020	92.5	18.30	< 0.01	0.004	5950.0	0.004	4.13	4360	0.170	119	11.9
BED15	4	15.00	bedrock	2.45	2.51	839	55.7	5.78	< 0.01	0.020	1580.0	0.004	23.20	953	0.110	55	7.8
LAT9a	5	0.20	dark red horizon	5.25	< 0.01	> 10000	61.3	49.10	< 0.01	0.001	7890.0	0.024	0.61	1750	0.111	300	29.9
LAT9b	5	1.50	red horizon	4.20	< 0.01	> 10000	90.0	49.40	< 0.01	0.001	> 10000	0.007	0.61	3850	0.062	340	18.9
LAT9c	5	2.50	yellow horizon	3.73	< 0.01	> 10000	116.0	49.10	< 0.01	0.001	> 10000	0.005	0.62	3110	0.059	375	11.6
LAT10a	6	0.10	dark red horizon	4.58	0.02	> 10000	49.3	34.90	< 0.01	0.003	6390.0	0.009	2.08	5530	0.067	604	10.8
LAT10b	6	1.00	red horizon	8.25	0.01	> 10000	32.0	33.80	< 0.01	0.003	3750.0	0.008	3.22	2740	0.068	740	10.0
LAT10c	6	1.50	red horizon	8.29	< 0.01	> 10000	33.2	32.90	< 0.01	0.003	4220.0	0.008	3.38	3100	0.077	753	11.8
LAT10d	6	2.50	yellow horizon	2.17	0.14	> 10000	106.0	40.90	0.01	0.004	> 10000	0.003	2.25	7910	0.043	589	4.1
LAT10e	6	3.50	saprolite	3.26	0.04	9560	63.4	21.80	0.07	0.016	> 10000	0.003	8.26	6850	0.082	954	9.6
BED18 weathered	6	4.00	bedrock	0.59	0.70	2850	24.7	7.50	< 0.01	0.006	3060.0	< 0.001	> 30.0	934	0.006	98	0.6
BED18 unweathered	6	4.00	bedrock	0.47	0.71	1960	31.9	5.98	< 0.01	0.004	2140.0	< 0.001	> 30.0	971	0.005	55	0.8

b

Sample ID	Profile No.	Profile depth [m]	Laterite horizon	Al	Ca	Cr	Fe	K	Na	Ni	P	Mg	Mn	Ti	Si	LOI
				%	%	%	%	%	%	%	%	%	%	%	%	%
LAT2	1	0.40	dark red horizon	2.70	0.16	1.59	39.34	0.00	0.02	0.89	0.00	5.28	0.68	0.05	6.91	10.29
LAT3	1	1.00	yellow horizon	2.74	0.01	1.66	41.23	0.00	0.00	0.96	0.00	0.78	0.72	0.05	9.05	10.82
LAT4	1	1.50	yellow horizon	3.92	0.01	2.03	47.75	0.00	0.00	0.94	0.00	0.66	0.30	0.10	2.90	12.72
LAT5	1	2.20	yellow horizon	2.06	0.00	1.02	26.68	0.00	0.00	0.79	0.00	1.00	0.59	0.03	21.25	7.65
SAP1	1	4.00	saprolite	0.28	0.30	0.54	7.04	0.00	0.00	2.57	0.00	18.21	0.11	0.01	21.97	7.51
SAP2*	1	4.00	saprolite	0.20	0.02	0.13	2.13	0.01	0.00	0.44	0.00	2.40	0.04	0.00	41.35	2.51
BED8 weathered	1	8.00	bedrock	0.58	1.05	0.45	6.97	0.00	0.00	0.45	0.00	25.36	0.11	0.01	20.42	0.32
BED8 unweathered	1	8.00	bedrock	0.49	1.01	0.37	6.32	0.00	0.00	0.24	0.00	26.47	0.11	0.01	20.57	-
LAT6a	2	0.10	dark red horizon	4.47	-	1.93	48.18	-	-	0.96	0.01	0.62	0.71	0.18	2.30	11.97
LAT6b	2	2.00	red horizon	3.35	0.02	1.90	49.67	0.01	-	0.99	0.01	0.79	0.89	0.12	2.44	11.19
SAP3 weathered	2	2.50	saprolite	1.62	1.80	0.50	6.98	0.00	0.06	1.08	0.00	19.62	0.09	0.06	19.91	6.98
SAP3 unweathered	2	2.50	saprolite	1.33	1.98	0.36	5.52	0.00	0.05	0.55	0.00	21.13	0.09	0.05	19.93	7.62
BED9	2	3.50	bedrock	0.08	0.01	0.37	6.16	0.00	0.00	0.27	0.00	22.29	0.10	0.01	18.63	13.20
LAT7a	3	0.30	dark red horizon	2.45	0.65	0.93	12.62	0.06	0.04	1.13	0.00	10.47	0.21	0.10	21.51	9.09
LAT7b	3	1.00	yellow horizon	1.96	0.75	1.12	15.67	0.04	0.00	1.06	0.00	9.26	0.30	0.05	21.06	8.46
BED12	3	8.00	bedrock	0.58	0.55	0.57	5.51	0.00	0.00	0.21	0.00	24.64	0.09	0.01	19.43	6.60
LAT8c	4	0.05	dark red horizon	5.26	0.59	1.16	17.19	0.02	0.03	0.46	0.01	6.08	0.79	0.23	16.65	15.43
LAT8a	4	0.40	red horizon	5.20	0.53	0.88	20.90	0.01	0.04	0.59	0.01	7.63	0.49	0.24	15.58	10.61
LAT8b	4	1.20	yellow horizon	4.51	0.35	0.73	21.58	0.01	0.00	0.67	0.00	3.12	0.21	0.19	19.12	11.69
BED15	4	15.00	bedrock	3.40	3.33	0.23	6.64	0.00	0.00	0.17	0.01	17.80	0.09	0.15	17.80	10.82
LAT9a	5	0.20	dark red horizon	3.85	0.01	3.07	50.07	0.00	0.00	0.75	0.01	0.52	0.17	0.11	0.93	13.14
LAT9b	5	1.50	red horizon	3.16	0.01	2.16	51.53	0.00	0.01	0.99	0.00	0.53	0.39	0.07	0.81	13.16
LAT9c	5	2.50	yellow horizon	3.21	0.00	2.22	51.55	0.00	0.00	0.97	0.00	0.57	0.34	0.07	0.79	13.05
LAT10a	6	0.10	dark red horizon	5.09	0.01	9.02	36.08	0.00	0.00	0.60	0.00	1.72	0.53	0.08	4.69	13.35
LAT10b	6	1.00	red horizon	6.34	-	11.51	38.88	0.02	-	0.43	0.01	2.31	0.29	0.08	3.09	7.21
LAT10c	6	1.50	red horizon	6.90	0.01	13.10	36.67	0.00	0.01	0.46	0.00	3.03	0.29	0.09	2.57	7.16
LAT10d	6	2.50	yellow horizon	3.46	0.14	2.88	42.83	0.02	0.00	1.58	0.00	2.08	0.86	0.05	4.40	12.38
LAT10e	6	3.50	saprolite	2.09	0.11	1.38	26.87	0.05	-	1.42	-	5.99	0.82	0.05	16.09	8.39
BED18 weathered	6	4.00	bedrock	0.44	0.60	0.43	7.12	0.00	0.00	0.37	0.00	25.90	0.11	0.01	20.51	0.11
BED18 unweathered	6	4.00	bedrock	0.34	0.52	0.36	6.20	0.00	0.00	0.26	0.00	27.29	0.10	0.01	20.46	-

Figures

Fig. 1a) Location of Lake Towuti on the island of Sulawesi, Indonesia. **b**) Geologic map of the Malili lake system with Lake Towuti and upstream Lakes Mahalona and Matano, modified after Costa et al. (2015). **c**) Map of the sampling locations around Lake Towuti; data for river bedload (squares) from Costa et al. (2015). **d**) Map of Lake Towuti, with river names and sampling locations. Red circles indicate the three coring sites of the ICDP Towuti Drilling Project

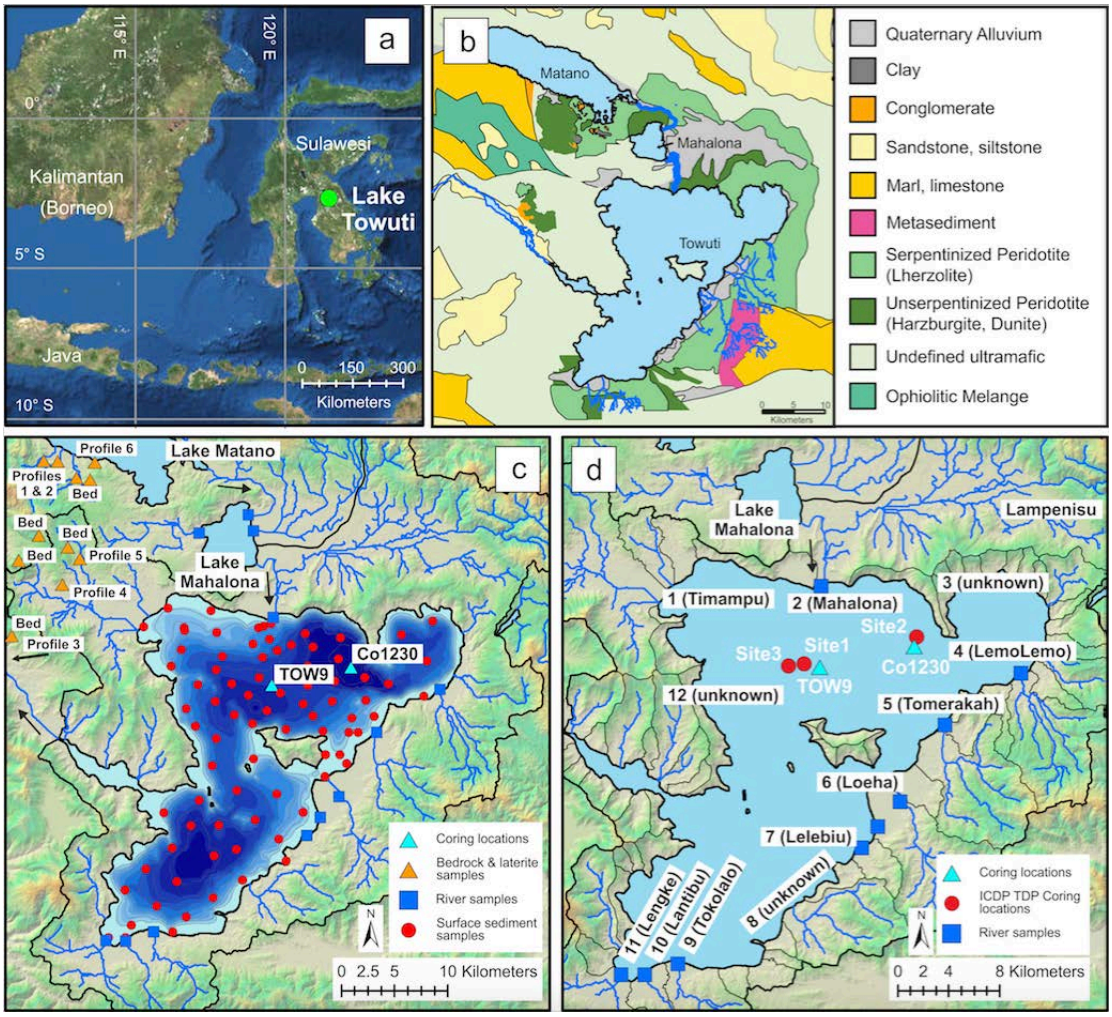

Fig. 2 Slope angles [°] in the Lake Towuti catchment. Colour classification is partly based on the critical angle of internal friction as determined in direct shearing tests on the sampled laterite material (26.5° and 43.79° for upper and lower laterite horizons, respectively). Slope data are based on the DEM. Insets: Long profiles of all major rivers flowing into Lake Towuti. Profiles are based on DEM analysis and were computed by the ArcGIS 10.1 hydrology toolset. (Color figure online)

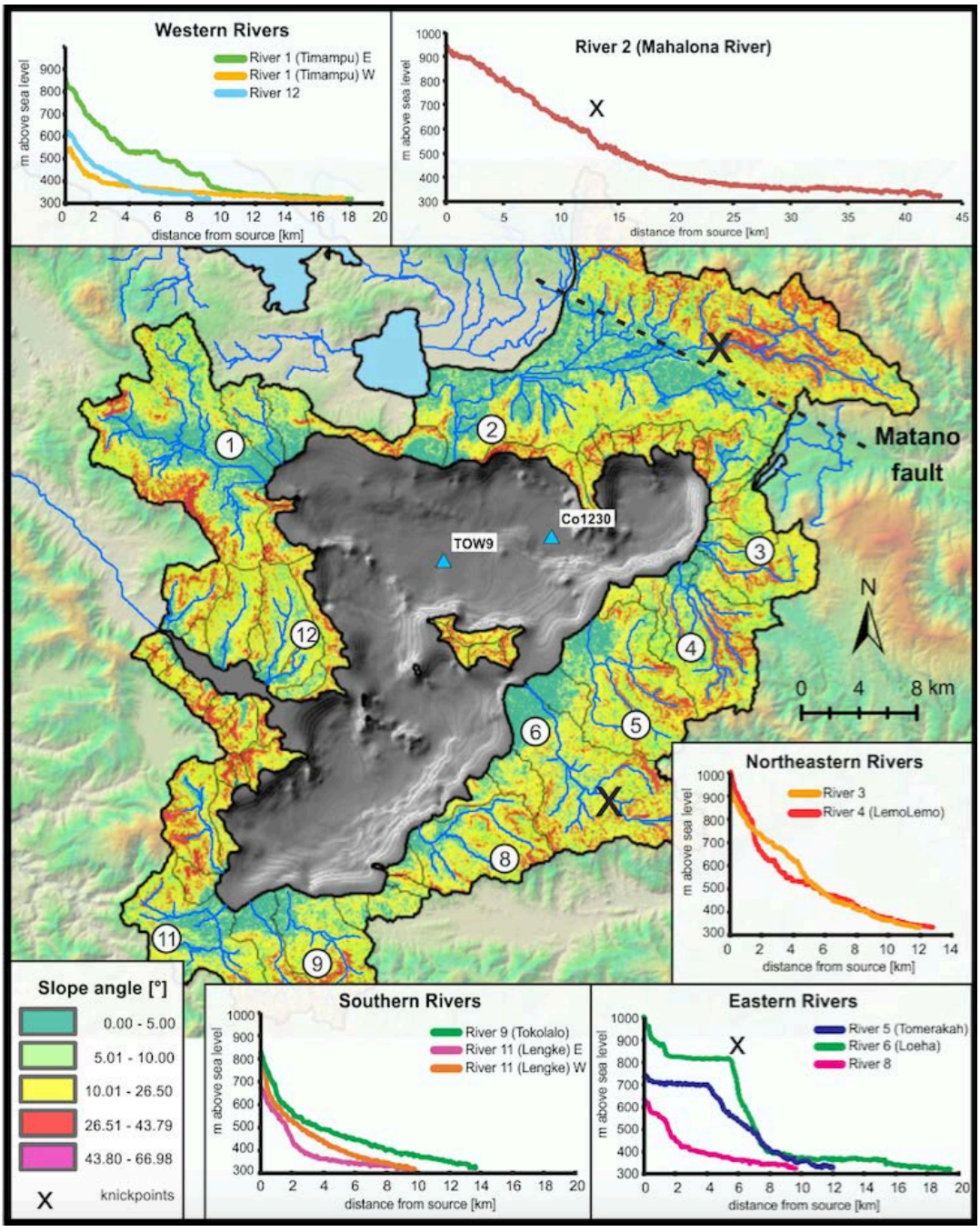

Fig. 3 Average element concentrations of six laterite profiles (for data from individual profiles, see Fig. S5). Depth is the average depth of each of the five zones. Error bars correspond to ± one standard deviation

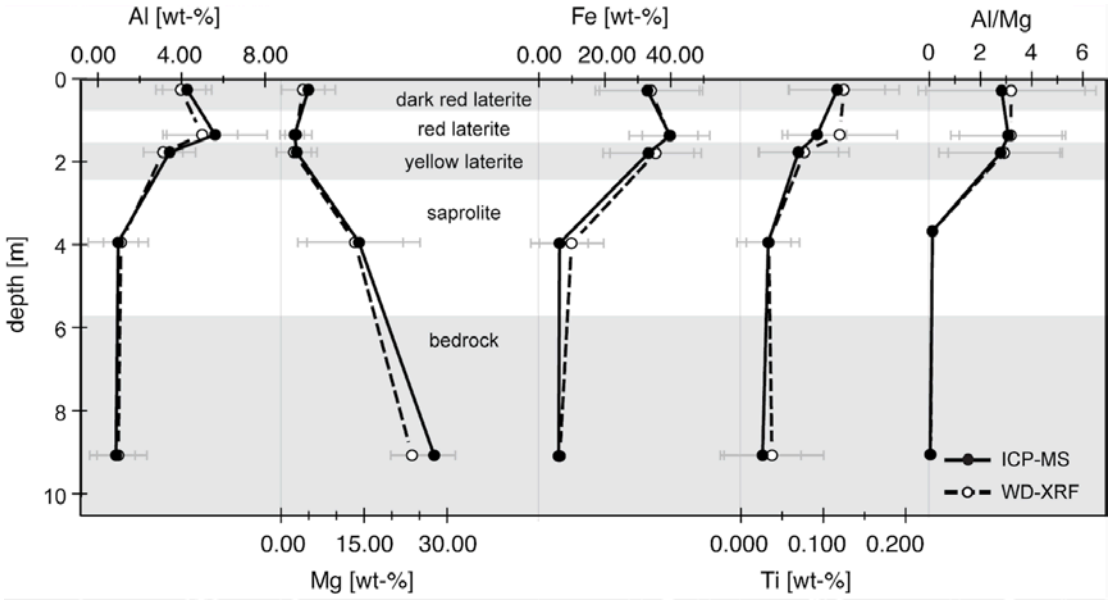

Fig. 4 a-d) Element concentrations of Al, Fe, Mg, and Ti determined by ICP-MS **e**) kaolinite-to-serpentine ratio determined by clay XRD and **f**) Al/Mg ratio determined by ICP-MS on 84 surface sediment samples, indicated by colour-coded circles. Background colouring is based on kriging interpolation of the surface sediment measurements. Grey lines represent the lake bathymetry with a 20-m line spacing (maximum water depth is ~200 m), data for river bedload (squares) from Costa et al. (2015), symbol size is scaled to catchment size (no data available for clay minerals). (Color figure online)

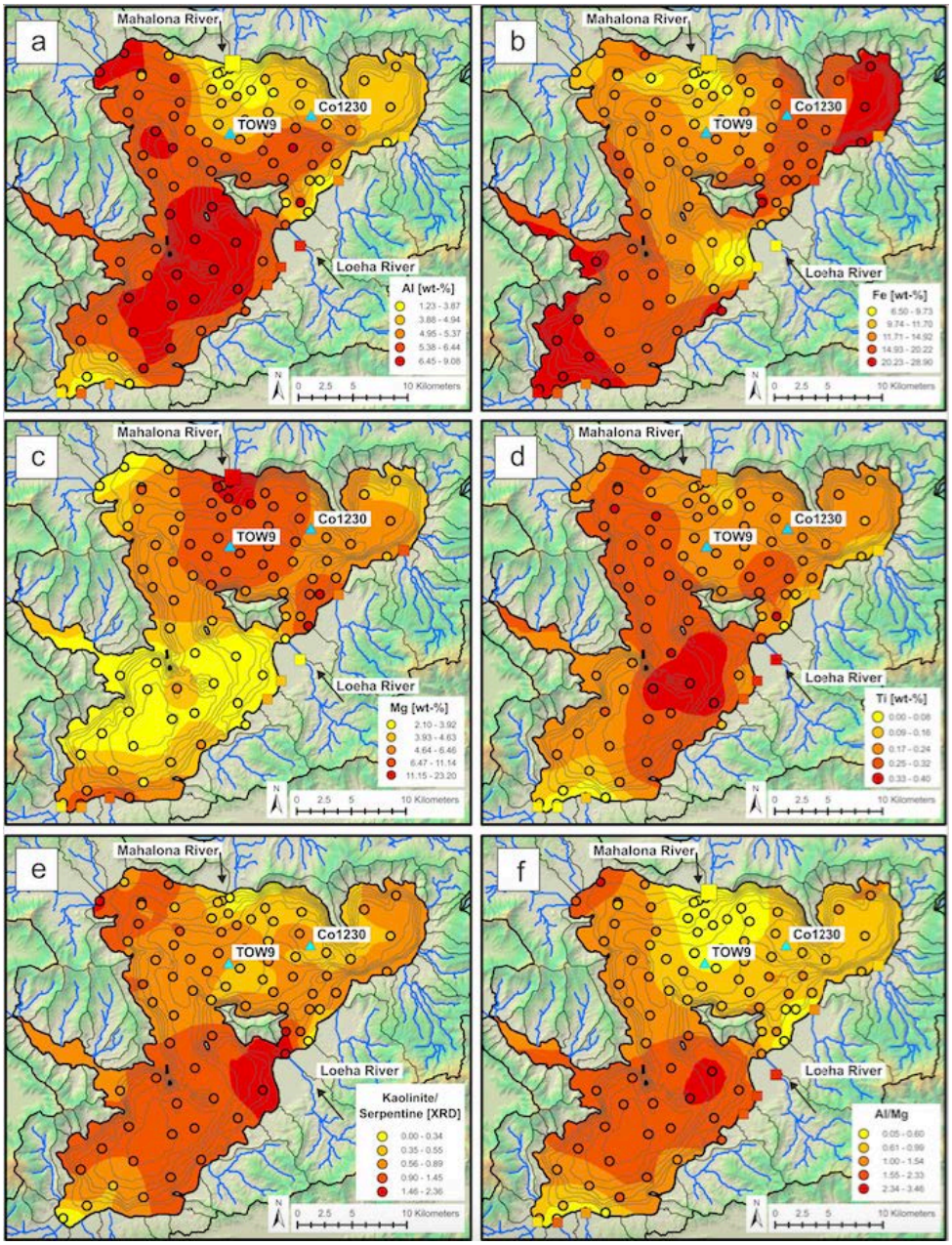

Fig. 5 a) Al/Mg ratio, **b**) Ti concentrations, **c**) kaolinite-to-serpentine ratio, and **d**) kaolinite content determined by clay XRD, of the two sediment cores, Co1230 and TOW9. The cores are located close to the two main sites of the ICDP Towuti Drilling Project (Fig. 1d). **e**) Mean daily insolation for March and September equinoxes at 2°S

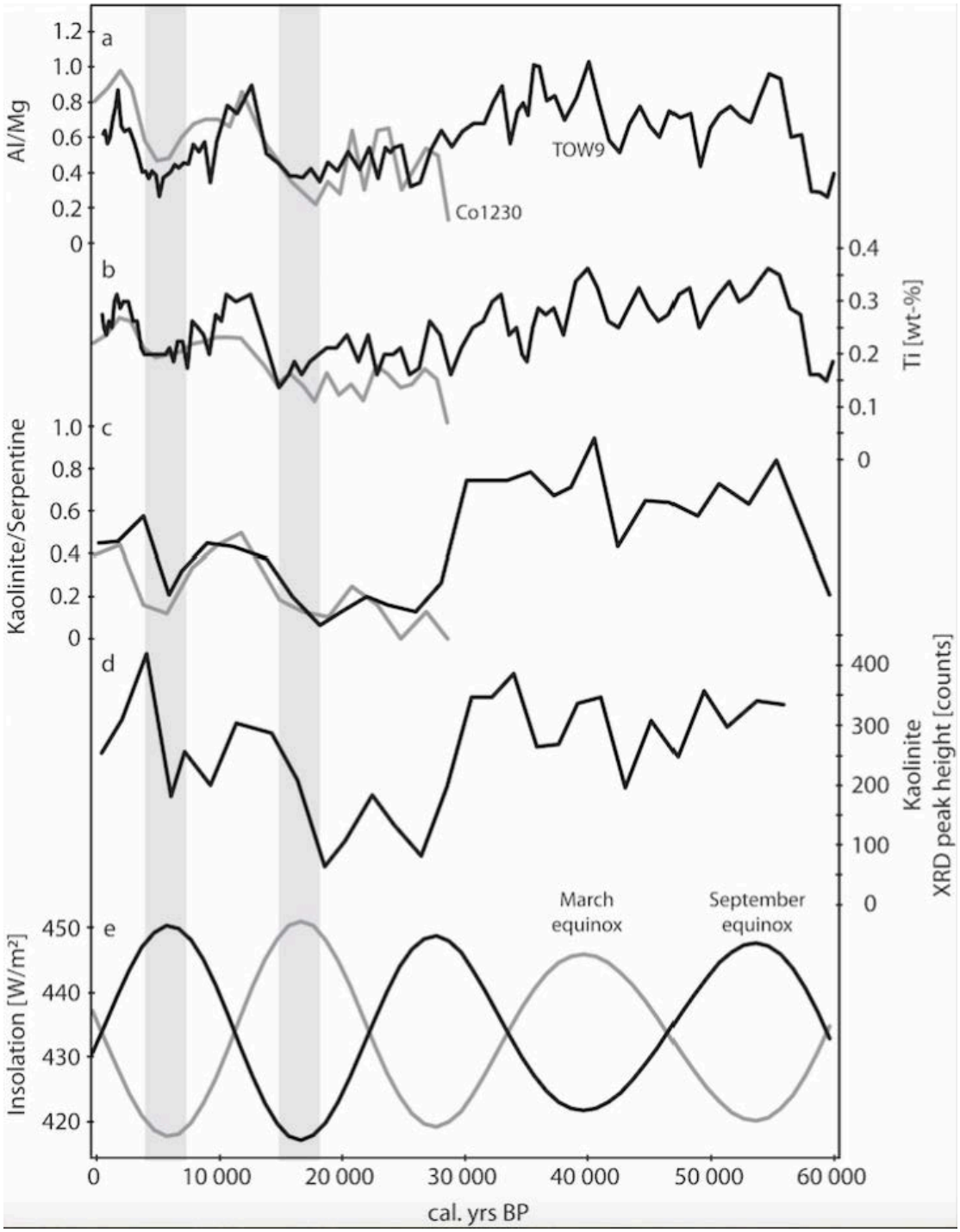

Electronic Supplementary Material

Fig. S1 a) Exemplary clay XRD spectra of a surface sediment sample with characteristic peaks for smectite (5.2° 2θ), illite (8.8° 2θ), serpentine (12.24° 2θ), and kaolinite (12.5° 2θ) in the ethylene glycol saturated sample. **b**) Correlation plots for surface sediment samples and **c**) for sediment core Co1230: comparison of clay-fraction XRD, clay-fraction mid-infrared FTIRS, and bulk Al and Mg. Correlation method and coefficients are indicated in the top left. Compared to MIR-FTIRS, XRD analysis on oriented clay separates to identify clay minerals in soils and lake sediments is more common. MIR-FTIRS has recently become an established method for the determination of the minerogenic and organic matter content of lake sediments (Rosén and Persson 2006), but is less commonly used for the identification of clay minerals in sediment records. Our results agree well with clay mineralogy analyses by Weber et al. (2015) and Goudge et al. (2017), who used near-infrared spectroscopy to determine the clay mineral content of a surface sediment transect and sediment cores from Lake Towuti. Our data thus show that XRD analysis on oriented clay separates as well as FTIR spectroscopy analysis reliably determine the clay mineralogical content of lake sediments from Towuti, in particular the amount of kaolinite and serpentine, whereas no reliable signal could be obtained for smectites and illite

Fig. S2 a) Average concentration of elements in the three laterite zones, in the saprolite, and in the bedrock. CIA calculation is based on Nesbitt and Young (1982). Colours indicate the five zones: unweathered parent rock (dark

green), saprolite zone (light green), and three laterite zones (orange, light red, dark red). Error bars correspond to ± one standard deviation. **b**) Element concentration of Al, Fe, Mg, and Ti for the six individual laterite profiles presented in this study. Concentrations were determined by ICP-MS, and vertical red lines indicate upper and lower detection limits where applicable. Bedrock type is indicated below the profiles. **c**) Kaolinite and serpentine concentrations in the laterite horizons based on diagnostic peak integration of FTIR spectra for kaolinite (wavenumbers 900.8-924.6 cm^{-1}; kaolinite 913) and serpentine (3674.9-3694.2 cm^{-1}; serpentine 3685) in absorption units

Fig. S3 Microscope images of bedrock thin sections. Left images are in unpolarised light, images to the right are in polarised light. Lowermost images show an olivine grain with a rind of serpentine and possibly magnetite

Fig. S4 Bulk XRD spectra for **a**) a laterite profile (profile 5) on top of unserpentinised peridotite bedrock, and **b**) a laterite profile (profile 4) on top of serpentinised peridotite bedrock

Fig. S5 Grain-size distribution curves for selected laterite samples based on settling (< 0.063 mm), wet (0.063, 0.125, 0.25 mm), and dry (0.5, 1, 2, 4 mm) sieving. Table indicates soil type categorized following the Unified Soil Classification System (USCS). Corresponding geotechnical parameters following Swiss Norm SN 670 010, and parameter values determined on the samples directly

Fig. S6 Maps of 84 surface sediment samples (colour-coded circles) with background colouring based on kriging interpolation and grey lines representing lake bathymetry with a 20-m line spacing (maximum water depth is ~200 m) for **a**) Median grain-size diameter (D50) determined by laser diffractometry ('topo-to-raster' interpolation tool was used for the interpolation), **b**) Chemical Index of Alteration (following Nesbitt and Young 1982), calculation based on ICP-MS measurements. **c-f**) Element concentrations of Ni, Cr, K, and Ca determined by ICP-MS analysis. **g**) Kaolinite-to-serpentine ratio determined by FTIRS, **h**) smectite-to-illite ratio determined by clay XRD. Light blue triangles show the location of the two sediment cores presented in this study, squares represent samples of river suspended load (symbol size is scaled to catchment size; data not available for all parameters)

Fig. S7 Bulk XRD spectra for a lake surface sediment transect from the Mahalona River mouth to the site of core TOW9 and TDP Site 1

Fig. S8 XY-plot and ternary diagram showing the element concentration of Al, Mg, and K (concentrations multiplied by 10) in bedrock, saprolite, laterite, river suspended load, surface sediments, and sediment core samples

ESM References

Rosén P, Persson P (2006) Fourier-transform Infrared Spectroscopy (FTIRS), a new method to infer past changes in tree-line position and TOC using lake sediment. J Paleolimnol 35: 913-923. DOI: 10.1007/s10933-005-5010-8)